Rapid and Multiplexed MicroRNA Diagnostic Assay Using Quantum Dot-Based Förster Resonance Energy Transfer

Xue Qiu and Niko Hildebrandt*

NanoBioPhotonics (nanofret.com), Institut d'Electronique Fondamentale, Université Paris-Sud/CNRS, 91405 Orsay Cedex, France

ABSTRACT The detection of next generation microRNA (miRNA) biomarkers has become a highly important aspect for clinical diagnostics. We use multiplexed Förster resonance energy transfer (FRET) between a luminescent Tb complex and three different semiconductor quantum dots (QDs) to sensitively detect three different miRNAs from a single 150 μL sample with *ca.* 1 nM (subpicomol) detection limits. The rapid and amplification-free mix-and-measure assay format is based on careful design of miRNA base pairing and stacking to selectively detect different miRNAs with very strong sequence homologies. Clinical applicability is demonstrated by sensitive multiplexed quantification of three miRNAs at low (2 to 10 nM) and varying concentrations in samples that contained up to 10% serum.

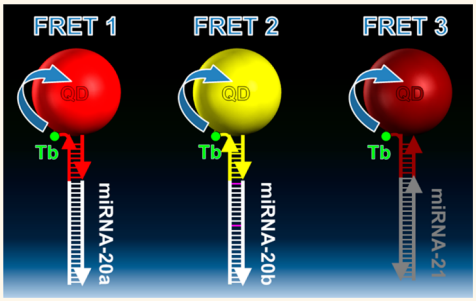

KEYWORDS: FRET · nanocrystals · miRNA · clinical diagnostics · terbium · multiplexing

To date, more than 30 000 microRNAs (miRNAs) have been discovered, of which more than 2500 can be found in humans.[1,2] Most of them are involved in tissue-specific gene expression control by acting as post-transcriptional repressors through binding to 3′-untranslated regions of target mRNA. Physiological homeostasis of cells and tissues is maintained by complex regulation, and therefore miRNA dysregulation can lead to diseases such as cancer or cardiovascular diseases.[3−6] As peripheral blood contains many different nucleic acids, a sensitive detection of circulating miRNA in plasma or serum could provide easily accessible genetic information and serve as next generation biomarker.[7−12] The importance of miRNA has led to the development of many different detection technologies,[13,14] among which quantitative reverse transcription-polymerase chain reaction (qRT-PCR), microarrays, nanostring technology, and small RNA sequencing are probably the most established strategies.[15] Although these methods can provide important advantages such as high sensitivity, high selectivity, or high throughput, a miRNA detection strategy that is ideally suited for clinical diagnostics does not exist to date. An ideal diagnostic miRNA assay should be single-step (*e.g.*, no washing and separation steps), sensitive (detection of low concentrations), specific (*e.g.*, discrimination of very similar sequences in complex mixtures), rapid (liquid phase binding kinetics and quick measurement), reproducible (low coefficients of variation), robust (stable sensing properties of bioconjugates), storable (*e.g.*, stable lyophilized bioconjugates within an assay kit format), easy to use (without complicated preparation procedures), versatile (generic format for many miRNAs as well as DNA, facile bioconjugate production/purification), and multiplexed (simultaneous measurement of several miRNAs).

The application of colloidal semiconductor quantum dots (QDs) in Förster resonance energy transfer (FRET)-based biosensing provides many advantages for the challenging diagnostic requirements, including high sensitivity (due to the brightness of QDs), multiplexing capability (due to the color tunability of QDs), and homogeneous assay formats (due to the biorecognition-specific

* Address correspondence to niko.hildebrandt@u-psud.fr.

Received for review June 3, 2015 and accepted July 20, 2015.

Published online July 20, 2015
10.1021/acsnano.5b03364

FRET signal).[16−18] In particular, we have shown that Tb-to-QD FRET immunoassays can fulfill the necessary requirements for diagnostic tests even in challenging media such as serum or plasma,[19] but multiplexed detection of different biomarkers from a single sample has not yet been demonstrated. We also developed Tb-to-QD FRET-based DNA hybridization assays,[20] but these utilized only a single QD color and the proof-of-principle system did not measure any free targets from a sample solution. Moreover, hybridization assays for the detection of the short (*ca.* 22 nucleotides) miRNAs are strongly limited in sensitivity because strand displacement assays (*e.g.*, using molecular beacons) need to overcome energy barriers,[21] and hybridization of two donor and acceptor oligos to a single short miRNA strand is not very stable at low concentrations. The advantages of QDs for FRET or fluorescence may become very useful for the detection of miRNA or other nucleic acids and recently several QD-based quantitative miRNA detection technologies have been developed.[22−32] However, none of these methods provided homogeneous single-step assays, only few could multiplex from a single sample, and high selectivity and sensitivity could only be realized by using enzymes (ligases, polymerases, or nucleases), amplification strategies, and complicated sensor designs (for a comparison of the different advantages and disadvantages of these technologies see Supporting Table S1). A multiplexed "mix-and-measure" technology would be highly desirable for quantitative miRNA diagnostics.

Here we present an enzyme-free, simple, rapid, and homogeneous multiplexed assay-technology for the sensitive detection of multiple miRNAs in a single small-volume buffer or serum-based sample measured at room temperature. The assay is based on time-gated FRET (TG-FRET) from the luminescent terbium complex Lumi4-Tb (Tb) to different commercial QDs.[34] It does neither require any washing or separation steps nor the addition of enzymes and has been designed for its application on an approved clinical diagnostics fluorescence microplate reader (KRYPTOR). In order to demonstrate full multiplexing functionality of our assay we have detected the three miRNAs hsa-miR-20a-5p, hsa-miR-20b-5p, and hsa-miR-21-5p in a single 150 μL sample at constant temperature, all with *ca.* 1 nM (subpmol) detection limits. We also demonstrate precise multiplexed measurements of these miRNAs at different and varying concentrations and the feasibility of adapting the technology to point-of-care testing (POCT) in buffer containing 10% serum. Our assay does not only demonstrate an important milestone for the integration of quantum dot nanoparticles to multiplexed clinical diagnostics but also a unique rapid miRNA detection technology that is complementary to the rather complicated high-throughput and high-sensitivity approaches that are established today.

RESULTS AND DISCUSSION

The recognition principle of the Tb and QD FRET probes and the miRNA biomarkers is based on RNA/DNA base pairing and stacking. As shown in Figure 1 the triplexed miRNA sensor is composed of three different QDs, with photoluminescence (PL) maxima at 605, 655, and 705 nm, respectively, that are conjugated with short DNA strands (7 or 8 nucleotides). These short DNA sequences are complementary to parts of three different reporter DNAs that are conjugated with Tb. However, the complementary sequences are too short to form stable double-strands by base pairing between the QD-DNA and the Tb-DNA (melting temperature $T_m \sim 20$ °C) and therefore Tb and QD are separated in solution (no FRET). The Tb-reporter DNAs were designed to provide a second sequence that is complementary to the three miRNAs hsa-miR-20a-5p (miRNA-20a), hsa-miR-20b-5p (miRNA-20b), and hsa-miR-21-5p (miRNA-21), respectively. Hybridization of the Tb-reporters to their respective miRNAs leads to stable double-stranded RNA/DNA ($T_m \sim 60$ °C) with a short overhang on the Tb-side. Due to RNA/DNA nick-based stacking this overhang can stably hybridize to the complementary QD-DNA,[33] which leads to the formation of three miRNA-specific double-stranded RNA/DNAs with distinguishable Tb-to-QD FRET pairs for PL-based detection (FRET 1 to 3). Sequences, modifications, labeling ratios and T_m values of all used oligonucleotides are summarized in Supporting Table S2. The extremely long PL lifetimes of Tb (milliseconds) allow efficient time-gated (TG) FRET detection from the same Tb to different QDs.[34] The TG PL detection (PL intensity integrated from 0.1 to 0.9 ms after the excitation pulse: I_{TG}) was performed in four different color detection channels to efficiently distinguish the FRET-sensitized QDs and the FRET-quenched Tb and to allow ratiometric measurements, in which the TG PL intensities of the QD-acceptors I_{TG}(QD) are divided by the TG PL intensities of the Tb-donors I_{TG}(Tb):

$$\text{FRETratio} = I_{TG}(\text{QD})/I_{TG}(\text{Tb}) \quad (1)$$

Because the specific formation of the different double-stranded RNA/DNA FRET complexes (FRET 1, 2, and 3) is based on both base pairing and stacking, a careful design and optimization of sequence lengths and orientations of the QD and Tb-DNAs was necessary to provide maximum selectivity and sensitivity for all three miRNA biomarkers. Too short QD-DNAs resulted in too weak base pairing and stacking interactions to form stable double-stranded RNA/DNA FRET complexes. Too long sequences led to stable hybridization of QD and Tb-DNA even without miRNA targets. The orientation (5′ to 3′ or *vice versa*) of the QD and Tb-DNAs was particularly important for the 20a and 20b sensors because of their sequence homology, which led to a strong orientation-dependent selectivity for

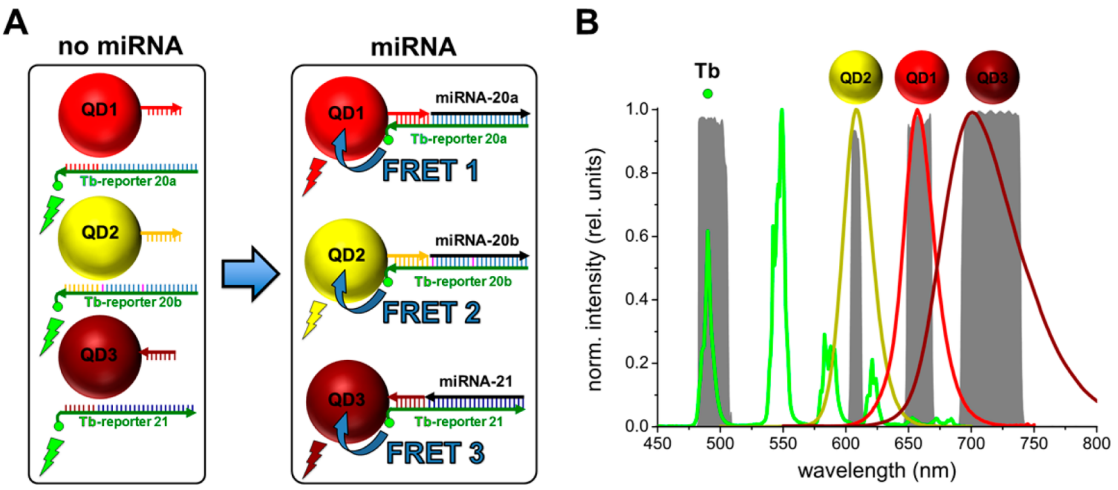

Figure 1. (A) The multiplexed mi-RNA assay is composed of three different QDs (QD1, 2, 3) that are conjugated with short DNA strands. These QD-DNAs are complementary (red, yellow, and brown color codes) to parts of three different Tb-conjugated DNA strands (Tb-reporter 20a, 20b, and 21). Base pairing of the complementary DNAs is not stable enough to form stable double-stranded DNA and therefore Tb and QDs are separated (left). Addition of the miRNAs 20a, 20b, and 21 leads to the formation of stable miRNA-Tb-reporter double-stranded RNA/DNAs, which can then hybridize to the short QD-DNAs due to the combination of base pairing and stacking. Only this combination leads to stable double-stranded RNA/DNAs, in which Tb and the different QDs are in close proximity to enable three different FRET processes (FRET 1, 2, and 3, right). Note: The Tb-reporter-miRNA double strands of 20a and 20b have only 2 base pair mismatches (magenta color code). Arrows point in 5′ to 3′ direction of the RNAs or DNAs. (B) The three FRET systems can be distinguished by the PL emission spectra of the QD acceptors, which are detected (together with the Tb PL spectrum) at different detection channels (gray spectra in the background).

miRNA-20a and 20b. Optimization of stacking effects using capture DNAs on the QDs with different lengths (Figure 2A) and of the orientation of these capture DNAs pointing in 3′-to-5′ direction from the QD or *vice versa* (Figure 2B) led to the selection of QD-DNAs with 8 bases for QD1 (miRNA-20a) and QD2 (miRNA-20b) with the 5′ end conjugated to the QD and to 7 bases for QD3 (miRNA-21) with the 3′ end conjugated to the QD. It should be noted that the optimization and choice of oligos were carried out for the assays to be performed at room temperature. However, our sensing approach can be implemented to a wider temperature range between *ca.* 10 and 37 °C. Lower and higher temperatures will result in stable FRET complexes even without miRNA and unstable FRET complexes even with miRNA, respectively.[35] For the calculation of T_m values we did not take into account changes due to attachment of the capture DNA to oligos, which may lead to an increased T_m.[26] However, even if the T_m values were slightly larger this was not problematic for our assays because our empiric optimization led to enhanced FRET sensitization in the presence of miRNA targets.

The next step of assay design was the selection of Tb-QD FRET pairs for the different miRNAs. Considering the Förster distances (9.0 nm for QD2, 10.7 nm for QD1, and 11.1 nm for QD3)[36] and the detection filter transmission bandwidth and Tb PL spectral crosstalk to the QD detection channels (Figure 1B) it was expected that the Tb-to-QD3 FRET pair (largest Förster distance and lowest Tb spectral crosstalk) would provide the highest sensitivity, followed by Tb-to-QD1 and Tb-to-QD2. MiRNA concentration-dependent measurements of the FRET ratios for all combinations of Tb-to-QD FRET pairs and miRNA sensors confirmed this assumption and also showed that the miRNA-20b sensor provided the highest sensitivity for all Tb-to-QD FRET pairs, followed by miRNA-20a and miRNA-21 (Supporting Figure S6). Therefore, the multiplexed sensor combined the strongest FRET pair with the weakest target-probe interaction and *vice versa* (*cf.* Figure 1A).

The performance of the single sensors is shown in Figure 3. In these assays the samples contained only one probe and one target at increasing concentrations. The FRET ratios of all three sensors increase nearly linearly with increasing miRNA concentrations between 0.5 and 10 nM (0.075 to 1.5 pmol), which was caused by QD FRET-sensitization from the Tb donors, as shown in the PL decay curves from the different QD detection channels (Figure 3 bottom graphs). Above this concentration range (the linear dynamic range for our probe concentration) the FRET ratios slowly leveled off and remained at a saturated value (plateau) after *ca.* 20 nM (data not shown), which was expected because this represents the concentration of the Tb-DNA and QD-DNA for target binding (saturation of the probe by the target). Within the FRET ratio curves (Figure 3 top graphs) it becomes obvious that the Tb-QD3 probe shows *ca.* one order magnitude lower FRET ratio intensities compared to Tb-QD1 and Tb-QD2 (although the relative FRET ratio increases are very similar). This behavior is caused by the much lower spectral crosstalk of Tb in the QD3 detection channel compared to QD1 and QD2 (*cf.* Figure 1B for spectral information and light green curves in the bottom graphs of Figure 3 for

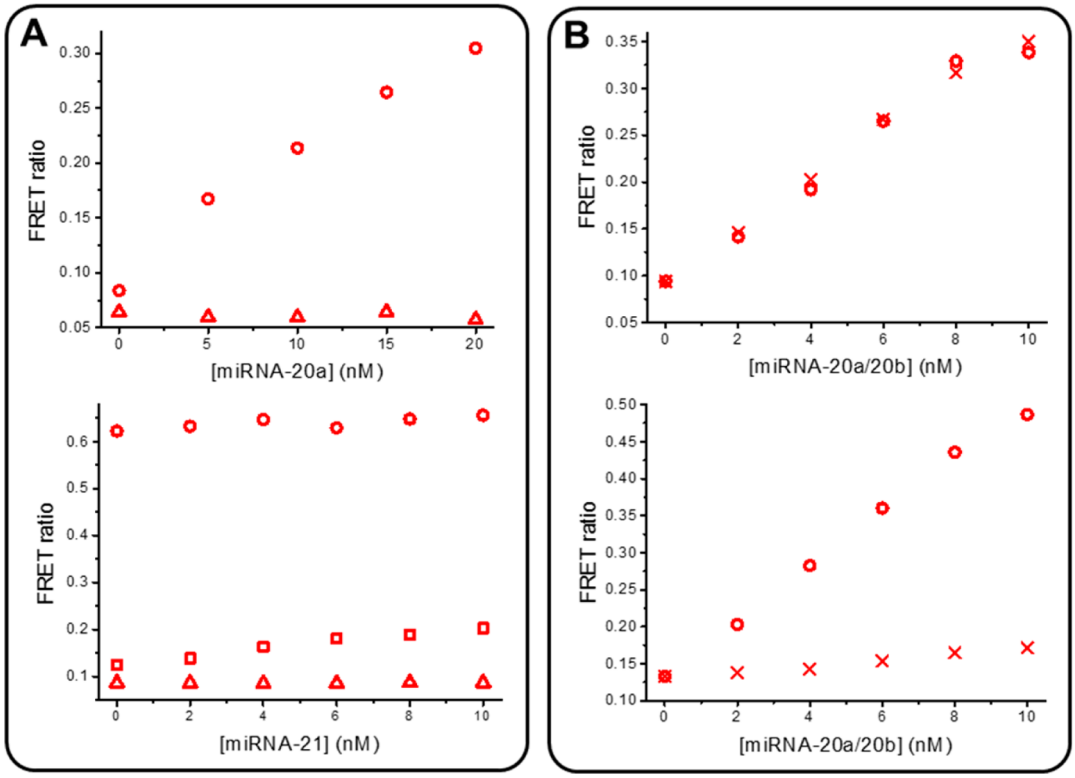

Figure 2. Concentration-dependent formation of double-stranded Tb-to-QD FRET RNA/DNA complexes (Figure 1A right) using different DNA lengths and orientations on QD1. (A) For the detection of miRNA-20a (top) and miRNA-21 (bottom) capture DNAs with 6 (triangles), 7 (squares), and 8 (circles) bases were applied. A 6-bases capture DNA does not lead to any FRET ratio increase with increasing miRNA concentration. An 8-bases capture DNA leads to a linear FRET ratio increase for the miRNA-20a probe but to a constant high FRET ratio for the miRNA-21 probe. For this probe a 7-bases capture DNA leads to linearly increasing FRET ratios. (B) Top: Using the miRNA-20a probe with QD1-DNA in 3′ to 5′ direction from the QD leads to an increasing FRET ratio with increasing concentrations of both miRNA-20a (circles) and miRNA-20b (crosses). Bottom: Inverting the QD-DNA direction (5′ to 3′ direction from the QD) leads to a significantly increasing FRET ratio with increasing concentrations of miRNA-20a, whereas the FRET ratios increase only slightly with increasing miRNA-20b concentrations. More details about the optimization of stacking and orientation effects can be found in Supporting Figures S2−S5.

intensity information). The FRET ratio (eq 1) is calculated by the time-gated QD intensities divided by the time-gated Tb intensities. The latter ones are very similar for all Tb-QD systems (same Tb concentration for all) but due to the lower Tb spectral crosstalk the QD3 intensities are significantly lower compared to QD1 and QD2. Another reason is the weaker probe-target interaction for miRNA-21 compared to miRNA-20a and 20b (*vide supra*), which also resulted in lower FRET ratio intensities (less FRET sensitization) and higher LODs although the Tb-QD3 FRET probe provides higher sensitivities for each miRNA when directly compared to the other two probes (Supporting Figure S6). Limits of detection (LODs) were estimated as the FRET ratio values on the calibration curves (Figure 3 top graphs) calculated from the FRET ratio of samples without miRNA plus three times their standard deviation (n = 30). The LODs were 0.12 nM (18 fmol), 0.06 nM (9.3 fmol), and 0.40 nM (60 fmol) for miRNA-20a, miRNA-20b, and miRNA-21, respectively.

Encouraged by the excellent performance of the single sensor assays we proceeded to an optimization for multiplexed miRNA detection, when all three probes and different amounts of the three miRNA targets were present into a single sample. We therefore prepared four different assays and three control samples (Figure 4). The first assay contained all three miRNAs at increasing concentrations from 2 to 10 nM (0.3 to 1.5 pmol). The second to fourth assay contained the same increasing concentrations but only of one of the three miRNAs. The three control samples contained high concentrations (10 nM) of two different miRNAs (20a + 20b, 20a + 21, or 20b + 21). As shown in Figure 4A and B miRNA-20a and miRNA-20b can be correctly detected almost completely independent of the concentrations of the other miRNAs in the samples. The presence of miRNA-20b shows a very small contribution to the miRNA-20a detection channel (difference between red and black data points) and *vice versa* (difference between dark-yellow and black data points), whereas the presence of miRNA-21 does not influence at all the detection of miRNA-20a and miRNA-20b. The detection of miRNA-21 in Figure 4C shows a different picture because the presence of both miRNA-20a and miRNA-20b strongly influences the quantification of miRNA-21. As discussed above the

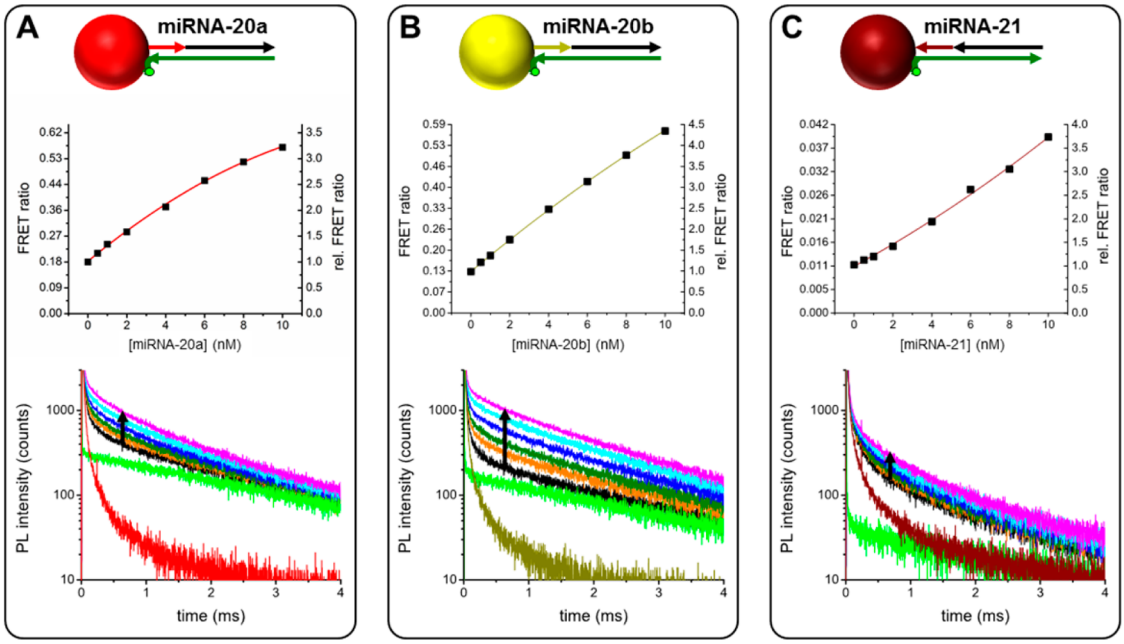

Figure 3. Performance evaluation of the single miRNA sensors (A: miRNA-20a, B: miRNA-20b, C: miRNA-21). The top graphs show the FRET ratios (eq 1) and rel. FRET ratios (FRET ratios normalized to unity at [miRNA] = 0) as a function of miRNA concentration. The nearly linear increase of these calibration curves is mainly caused by QD FRET-sensitization *via* long-lived (ms) excited states of Tb. This sensitization becomes obvious in the PL decay curves of the different QD detection channels (bottom graphs), in which the long-lifetime parts of the decay curves strongly increase with increasing miRNA concentrations (0 nM: black, 1 nM: orange, 2 nM: dark green, 4 nM: blue, 6 nM: cyan, 10 nM: magenta) as indicated by the black arrows. Control experiments with only Tb-DNA and 6 nM miRNA (light green) and only QD-DNA and 6 nM miRNA (color of the QD, dark-yellow for QD2 for better visibility) showed the background of Tb PL (spectral crosstalk in the QD detection channels) and directly excited QD PL.

absolute FRET ratio values (left ordinates in Figure 3) are much lower for miRNA-21. This strong difference in absolute intensities leads to a significant spectral crosstalk of QD1 and QD2 into the QD3 detection channel (which is not obvious from the intensity-normalized spectra from Figure 1B).

Using the miRNA concentration-dependent (linearly increasing) FRET ratios generated by the miRNA-20a and miRNA-20b sensors in the miRNA-21 detection channel (red and dark-yellow data points in Figure 4C) and the precise and selective quantification of these two miRNAs in their own detection channels (Figure 4A and B), the FRET ratio contribution of these two sensors to the miRNA-21 detection channel can be easily subtracted (*cf.* Supporting Information for the complete mathematical model). As shown in Figure 4D the mathematical correction leads to a similar selectivity for miRNA-21 as for the other two miRNAs. The LODs for the three miRNAs within the multiplexed assays (with all three sensors present) were estimated as the FRET ratio values on the calibration curves calculated from the FRET ratio of samples without miRNA plus three times their standard deviation (n = 30). To evaluate conditions in which all of the targets are present in the samples, the calibration curves for the different miRNAs (similar to those in Figure 4A, B, and D) were measured in the absence and in the presence of the other miRNA targets and the average LODs were estimated as 1.3 nM (190 fmol), 0.9 nM (130 fmol), and 0.7 nM (110 fmol) for miRNA-20a, miRNA-20b, and miRNA-21, respectively (*cf.* Table 1 for all values that led to the averaged LODs).

In a final evaluation step of our homogeneous multiplexed miRNA detection technology we challenged the assays with varying concentrations of the different miRNAs and with ambitious sample conditions. We therefore prepared nine different samples that contained between 2 and 10 nM (0.3 and 1.5 pmol) of the three miRNAs at varying concentrations (as found in real samples) in buffer and in samples containing 10% serum. In clinical diagnostics circulating miRNA is usually detected from blood or serum extracted RNA samples using commercially available extraction kits.[25] Detection directly in whole blood, serum, or plasma would avoid such extraction steps and lead to a simpler and faster assay format. Circulating miRNAs circumvent degradation by endogenous ribonucleases, most probably through protection by their association to exosomes or protein and lipid complexes,[37] and direct detection of circulating miRNAs may be possible. Such degradation cannot be avoided for exogenous miRNA and therefore our probes were preincubated with the miRNA targets to form DNA/RNA FRET complexes before their addition to the serum samples. The aim of our serum-based experiments was to demonstrate the biological, chemical, and photophysical stability of

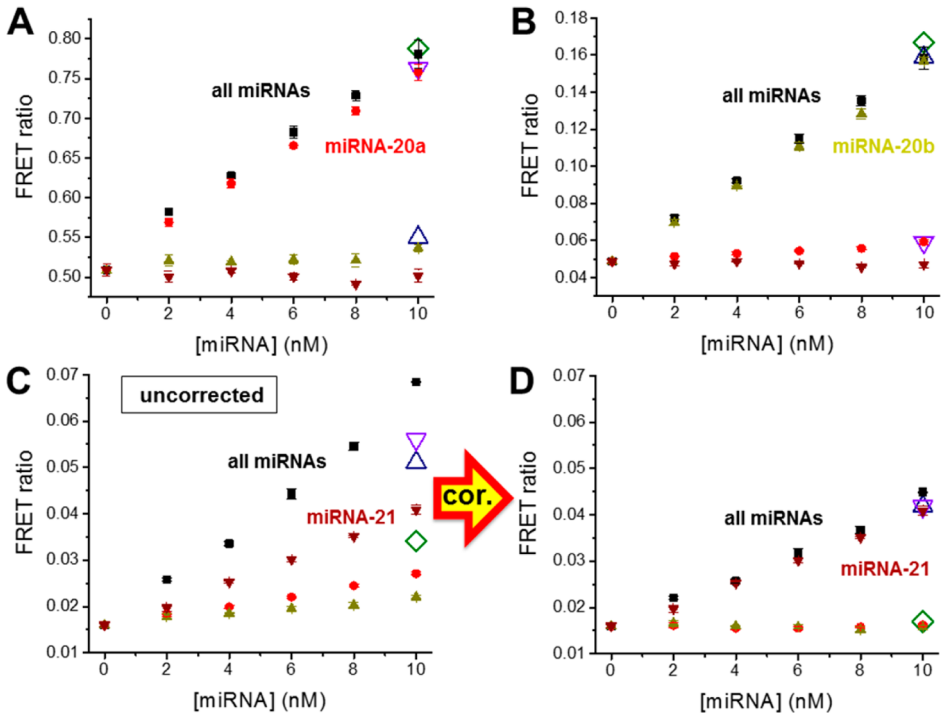

Figure 4. Multiplexed miRNA assays for the detection of miRNA-20a (A), miRNA-20b (B), and miRNA-21 (C and D). All assays contain all three sensors at constant concentrations and the different miRNAs at varying concentrations (as indicated on the abscissae). Black squares: all miRNAs; red dots: only miRNA-20a; dark-yellow upward triangles: only miRNA-20b; brown downward triangles: only miRNA-21. Open symbols present samples with 10 nM (1.5 pmol) of each miRNA-20a and miRNA-20b (green diamonds), miRNA-20b and miRNA-21 (blue upward triangles) and miRNA-20a and miRNA-21 (purple downward triangles). For miRNA-20a and miRNA-20b there are only minor differences between assays with single or multiple miRNAs. Quantification of miRNA-21 (C) is strongly influenced by the other two miRNAs and must therefore be corrected (D) to allow a specific and correct quantification of miRNA-21. The mathematical correction model is explained in the Supporting Information.

TABLE 1. Limits of Detection (LODs) of the Triplexed miRNA Assay (All Three Probes Are Present in the Samples) For the Three Different miRNAs under Different Conditions (with or without the Presence of Other Targets)

LODs	nM			fmol		
miRNA	20a	20b	21	20a	20b	21
X[a]	0.67	0.21	0.48	100	32	72
X + 10 nM Y	1.38	1.46	0.64	207	220	95
X + 10 nM Z	0.53	0.30	0.43	80	45	65
X + 10 nM Y + Z	2.50	1.54	1.38	375	231	207
Average	**1.27**	**0.88**	**0.73**	**190**	**132**	**110**

[a] If X = 20a then Y = 20b and Z = 21; if X = 20b then Y = 20a and Z = 21; if X = 21 then Y = 20a and Z = 20b.

our probe-target complexes and their sensitive and precise quantification in serum samples. Further investigations and in particular clinical studies using patient samples are necessary to verify if our approach can be used for direct measurements in serum and if the miRNA concentration range in such samples is sufficient to be quantified by our technique or if extraction of RNA from whole blood is required for their detection.

The FRET ratio calibration curves for the buffer and serum-based assays were determined by using an average of single miRNA and multiple miRNA curves because the latter showed small deviations from the single target calibration functions (*cf.* Supporting Figures S8 and S9). The calibration curves show a strong influence of serum on the Tb-QD3-miRNA-21 system, for which the absolute FRET ratio intensity decreased *ca.* 5-fold, whereas the other two sensors did not show significant changes between buffer and serum-based experiments. This is related to the weaker prehybridization of the miRNA-21 probe (QD-DNA capture and Tb-DNA reporter) without any miRNA inside the solution. This prehybridization consists of 7 base pairs for the miRNA-21 probe and of 8 base pairs for the miRNA-20a and 20b probes (see Supporting Table S2 for T_m values). This weaker capture-reporter interaction is therefore stronger influenced by the increased nuclease activity due to the addition of serum. Nevertheless, the most important aspect is the relative increase of the FRET ratio, which is not significantly affected by the addition of serum (because the full probe-target complexes are very stable—high T_m values) and therefore all three miRNAs can still be measured in a triplexed serum-containing assay. As shown in Figure 5 the various concentrations of the different miRNAs in both buffer and serum-based samples could be detected with quite high

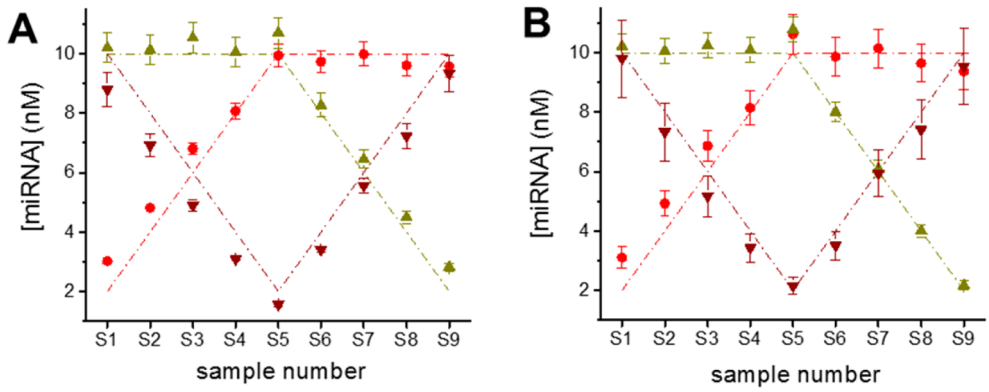

Figure 5. Triplexed homogeneous miRNA assay results for samples containing all three miRNAs at different concentrations between 2 nM (0.3 pmol) and 10 nM (1.5 pmol) in buffer (A) and in 10% serum (B). Red: miRNA-20a; dark-yellow: miRNA-20b; brown: miRNA-21. Dash-dotted lines represent know concentrations. Error bars of the measured data points resulted from triplicate measurements per sample and averaging from two different calibration curves (Supporting Figures S8 and 9).

precision at low nM concentrations (few pmol). MiRNA-20b can be measured with the highest precision with only minor deviations from the known concentration values. The combination of high miRNA-20b and low miRNA-20a concentrations led to an overestimation of miRNA-20a (due to miRNA-20b contributions in the miRNA-20a channel), which automatically led to an underestimation of miRNA-21 concentrations (overcorrection). Nevertheless, the concentration trends were extremely well detected, in particular when considering the simplicity of our correction model and the very challenging homogeneous assay (only 30 min of incubation, no washing and separation steps, and only 2.5 s of measurement per miRNA) with three different miRNAs (of which two have a strong sequence homology). It can be expected that automation of sample preparation and the application of more sophisticated models[38] can further improve the detection sensitivity.

CONCLUSION

We have developed a rapid and sensitive Tb-to-QD FRET-based miRNA assay that does not require any washing and separation steps (homogeneous) and can selectively detect three different miRNAs from a single 150 μL sample with detection limits down *ca.* 0.06 nM (9 fmol) for single sensor assays and *ca.* 0.2 nM (30 fmol) for triplexed assays. Immediate applicability to diagnostic applications was demonstrated by sensitive multiplexed measurements in samples that contained 10% serum. The assays work at room temperature on a clinically approved fluorescence plate reader system and do not require any amplification mechanisms such as PCR. Only 30 min of sample incubation and 7.5 s of measurement are required to selectively quantify three different miRNAs at varying concentrations down to 2 nM (0.3 pmol). This multiplexed assay exploits the unique properties of QD nanocrystals and demonstrates their applicability in multiplexed diagnostics. The homogeneous and sensitive multitarget miRNA test presents an important complementary technique to existing detection approaches that offer ultrahigh sensitivity (*e.g.*, PCR) or high throughput (*e.g.*, microarrays) but very complicated technologies, and it provides the unique potential for rapid miRNA clinical diagnostics.

MATERIALS AND METHODS

Materials. Lumi4-Tb-NHS was provided by Lumiphore, Inc. Water was purified by Purelab Option-Q equipped with biofilter (ELGA LabWater). Oligonucleotides were purchased HPLC purified from Eurogentec. All sequences and modifications of nucleic acids used in this study are summarized in Table S2. Qdot 605/655/705 ITK Streptavidin Conjugate Kits and Zeba Spin Desalting Columns (7 kDa MWCO) were purchased from Thermo Fisher Scientific. Tris(hydroxymethyl)-aminomethane, bovine serum albumin, and HEPES were purchased from Sigma-Aldrich. NaCl was purchased from Duchefa. Newborn calf serum was provided by Cezanne/Thermo Fisher Scientific.

Tb and QD DNA Conjugates. QD-DNA conjugates were obtained by mixing QD605-sAv/QD655-sAv/QD705-sAv with biotin-labeled oligonucleotides in hybridization buffer (20 mM Tris-Cl, 500 mM NaCl, pH 8.0) just before use. Tb-DNA conjugates were obtained by mixing Lumi4-Tb-NHS (lyophilized product dissolved to 8 mM in anhydrous DMF) in concentration excess to amino-functionalized oligonucleotides in 100 mM carbonate buffer at pH 9.0. The mixtures were incubated while rotating at 30 rpm (Intelli-Mixer, ELMI) overnight at room temperature. The Tb-DNA conjugates were purified 3 times by Zeba Spin Desalting Columns (7 kDa MWCO). Tb concentrations were determined by absorbance measurements at 340 nm using a molar absorptivity of 26 000 M^{-1} cm^{-1} as provided by the manufacturer. DNA was quantified by absorbance measurements at 260 nm. Labeling ratios (Table S2) were determined by linear combination of the respective absorbance values of Tb and oligo within the Tb-oligo conjugates.

Photophysical Properties. Absorption spectra (Lambda 35 UV/vis System, PerkinElmer) and emission spectra (FluoTime 300, PicoQuant) were recorded in HEPES (100 mM, pH 7.4) and hybridization buffer for Tb and QD samples, respectively. PL decay curves were acquired on a fluorescence plate reader (Edinburgh Instruments) using 4000 detection bins of 2 μs integration time and nitrogen laser (MNL 100, LTB Lasertechnik Berlin) excitation (337.1 nm, 20 Hz). Optical transmission filter

bandpass wavelengths were (494 ± 20) nm (Semrock) for the Tb detection channel, (607 ± 8) nm (Delta) for the QD2 detection channel, (660 ± 13) nm (Semrock) for the QD1 detection channel, and (716 ± 40) nm (Semrock) for the QD3 detection channel.

miRNA Assays. Time-gated (0.1−0.9 ms) PL intensity measurements were acquired on a KRYPTOR compact plus clinical fluorescence plate reader (Cezanne/Thermo Fisher Scientific) using the same Tb and QD detection channel bandpass filters as mentioned above. All FRET-assays were measured in black 96-well microtiter plates with an optimal working volume of 150 μL. All samples are prepared in hybridization buffer and contained 0.5 nM of each QD-DNA (prepared by mixing 0.5 nM QD-sAv and 20 nM biotinylated DNA just before the addition of the other constituents), 20 nM of each Tb-DNA, and increasing concentrations of miRNAs. The single sensor assays contained only one type of QD-DNA and Tb-DNA. After sample preparation they were incubated in the microtiter plates for 30 min at room temperature (22 °C) before measurements. In the single sensor assays each measurement consisted of 100 excitation flashes at 20 Hz repetition rate (5 s per measurement). In the multiplexed assays each measurement consisted of 50 excitation flashes at 20 Hz repetition rate (2.5 s per miRNA, 7.5 s for three miRNAs). For statistical analysis and the estimation of LODs all samples were prepared 3 times and measured in triplicates (n = 9) apart from the zero-concentration samples (without miRNA targets), which were prepared 10 times and measured in triplicates (n = 30). Samples of miRNA assays with varying target concentrations in buffer and buffer containing 10% newborn calf serum were prepared 3 times and measured once (n = 3). The serum was added after preincubation of sensor and targets for 15 min.

Conflict of Interest: The authors declare no competing financial interest.

Acknowledgment. The authors thank Lumiphore, Inc. for the gift of Lumi4-Tb-NHS reagents, the European Union (Innovative Medicines Initiative project OncoTrack) for financial support, and the Chinese Scholarship Council (CSC) for funding the PhD fellowship of X.Q.

Supporting Information Available: Comparison of the different advantages and disadvantages of QD-based miRNA detection technologies (Table S1), overview of oligonucleotide properties, Tb-to-oligo conjugation ratios, and melting temperatures (Table S2), RNA/DNA stacking effects (Figures S1 and S2), RNA/DNA orientation effects (Figures S3, S4, and S5), optimized sensor designs for the three miRNAs and three QDs (Figure S6), mathematical model of spectral crosstalk correction (Figure S7), and FRET ratio calibration curves in buffer and serum samples (Figures S8 and S9). The Supporting Information is available free of charge on the ACS Publications website at DOI: 10.1021/acsnano.5b03364.

REFERENCES AND NOTES

1. Kozomara, A.; Griffiths-Jones, S. MiRBase: Annotating High Confidence MicroRNAs Using Deep Sequencing Data. *Nucleic Acids Res.* **2014**, *42*, D68–73.
2. *The microRNA Database*, http://www.mirbase.org/cgi-bin/browse.pl?org=hsa. (Accessed on: May 2015).
3. Iorio, M. V.; Croce, C. M. MicroRNA Dysregulation in Cancer: Diagnostics, Monitoring and Therapeutics. A Comprehensive Review. *EMBO Mol. Med.* **2012**, *4*, 143–159.
4. Pencheva, N.; Tavazoie, S. F. Control of Metastatic Progression by MicroRNA Regulatory Networks. *Nat. Cell Biol.* **2013**, *15*, 546–554.
5. Esquela-Kerscher, A.; Slack, F. J. Oncomirs - MicroRNAs with a Role in Cancer. *Nat. Rev. Cancer* **2006**, *6*, 259–269.
6. Calin, G. A.; Croce, C. M. MicroRNA Signatures in Human Cancers. *Nat. Rev. Cancer* **2006**, *6*, 857–866.
7. Dong, Y.; Wu, W. K. K.; Wu, C. W.; Sung, J. J. Y.; Yu, J.; Ng, S. S. M. MicroRNA Dysregulation in Colorectal Cancer: A Clinical Perspective. *Br. J. Cancer* **2011**, *104*, 893–898.
8. Frampton, A. E.; Gall, T. M.; Castellano, L.; Stebbing, J.; Jiao, L. R.; Krell, J. Towards a Clinical Use of MiRNAs in Pancreatic Cancer Biopsies. *Expert Rev. Mol. Diagn.* **2013**, *13*, 31–34.
9. Weiland, M.; Gao, X.-H.; Zhou, L.; Mi, Q.-S. Small RNAs Have a Large Impact: Circulating MicroRNAs as Biomarkers for Human Diseases. *RNA Biol.* **2012**, *9*, 850–859.
10. Lu, J.; Getz, G.; Miska, E. A.; Alvarez-Saavedra, E.; Lamb, J.; Peck, D.; Sweet-Cordero, A.; Ebert, B. L.; Mak, R. H.; Ferrando, A. A.; *et al.* MicroRNA Expression Profiles Classify Human Cancers. *Nature* **2005**, *435*, 834–838.
11. Rosenfeld, N.; Aharonov, R.; Meiri, E.; Rosenwald, S.; Spector, Y.; Zepeniuk, M.; Benjamin, H.; Shabes, N.; Tabak, S.; Levy, A.; *et al.* MicroRNAs Accurately Identify Cancer Tissue Origin. *Nat. Biotechnol.* **2008**, *26*, 462–469.
12. Schwarzenbach, H.; Pantel, K. Circulating MicroRNAs as Non-Invasive Biomarkers. In *MicroRNAs in Medicine*; John Wiley & Sons: Hoboken, NJ, 2014; pp 567−588.
13. de Planell-Saguer, M.; Rodicio, M. C. Analytical Aspects of MicroRNA in Diagnostics: A Review. *Anal. Chim. Acta* **2011**, *699*, 134–152.
14. de Planell-Saguer, M.; Rodicio, M. C. Detection Methods for MicroRNAs in Clinic Practice. *Clin. Biochem.* **2013**, *46*, 869–878.
15. Mestdagh, P.; Hartmann, N.; Baeriswyl, L.; Andreasen, D.; Bernard, N.; Chen, C.; Cheo, D.; D'Andrade, P.; DeMayo, M.; Dennis, L.; *et al.* Evaluation of Quantitative MiRNA Expression Platforms in the MicroRNA Quality Control (miRQC) Study. *Nat. Methods* **2014**, *11*, 809–815.
16. Hildebrandt, N.; Wegner, K. D.; Algar, W. R. Luminescent Terbium Complexes: Superior Förster Resonance Energy Transfer Donors for Flexible and Sensitive Multiplexed Biosensing. *Coord. Chem. Rev.* **2014**, *273−274*, 125–138.
17. Geißler, D.; Lindén, S.; Liermann, K.; Wegner, K. D.; Charbonnière, L. J.; Hildebrandt, N. Lanthanides and Quantum Dots as Förster Resonance Energy Transfer Agents for Diagnostics and Cellular Imaging. *Inorg. Chem.* **2014**, *53*, 1824–1838.
18. Algar, W. R.; Kim, H.; Medintz, I. L.; Hildebrandt, N. Emerging Non-Traditional Förster Resonance Energy Transfer Configurations with Semiconductor Quantum Dots: Investigations and Applications. *Coord. Chem. Rev.* **2014**, *263−264*, 65–85.
19. Wegner, K. D.; Jin, Z.; Lindén, S.; Jennings, T. L.; Hildebrandt, N. Quantum-Dot-Based Förster Resonance Energy Transfer Immunoassay for Sensitive Clinical Diagnostics of Low-Volume Serum Samples. *ACS Nano* **2013**, *7*, 7411–7419.
20. Algar, W. R.; Wegner, D.; Huston, A. L.; Blanco-Canosa, J.-B.; Stewart, M. H.; Armstrong, A.; Dawson, P. E.; Hildebrandt, N.; Medintz, I. L. Quantum Dots as Simultaneous Acceptors and Donors in Time-Gated Förster Resonance Energy Transfer Relays: Characterization and Biosensing. *J. Am. Chem. Soc.* **2012**, *134*, 1876–1891.
21. Baker, M. B.; Bao, G.; Searles, C. D. *In Vitro* Quantification of Specific MicroRNA Using Molecular Beacons. *Nucleic Acids Res.* **2012**, *40*, e13.
22. Zhang, Y.; Zhang, C. Y. Sensitive Detection of MicroRNA with Isothermal Amplification and a Single-Quantum-Dot-Based Nanosensor. *Anal. Chem.* **2012**, *84*, 224–31.
23. Zeng, Y. P.; Zhu, G.; Yang, X. Y.; Cao, J.; Jing, Z. L.; Zhang, C. Y. A Quantum Dot-Based MicroRNA Nanosensor for Point Mutation Assays. *Chem. Commun.* **2014**, *50*, 7160–7162.
24. Geng, Y.; Lin, D. J.; Shao, L. J.; Yan, F.; Ju, H. X. Cellular Delivery of Quantum Dot-Bound Hybridization Probe for Detection of Intracellular Pre-MicroRNA Using Chitosan/Poly(γ−Glutamic Acid) Complex as a Carrier. *PLoS One* **2013**, *8*, e65540.
25. Jou, A. F. J.; Lu, C. H.; Ou, Y. C.; Wang, S. S.; Hsu, S. L.; Willner, I.; Ho, J. A. A. Diagnosing the MiR-141 Prostate Cancer Biomarker Using Nucleic Acid-Functionalized CdSe/ZnS QDs and Telomerase. *Chem. Sci.* **2015**, *6*, 659–665.
26. Song, W.; Qiu, X.; Lau, C.; Lu, J. Quantum Dot-Enhanced Detection of Dual Short RNA Sequences *via* One-Step Template-Dependent Surface Hybridization. *Anal. Chim. Acta* **2012**, *735*, 114–20.
27. Zhang, H.; Liu, Y.; Fu, X.; Yuan, L.; Zhu, Z. Microfluidic Bead-Based Assay for MicroRNAs Using Quantum Dots as Labels and Enzymatic Amplification. *Microchim. Acta* **2015**, *182*, 661–669.

28. Liang, R. Q.; Li, W.; Li, Y.; Tan, C. Y.; Li, J. X.; Jin, Y. X.; Ruan, K. C. An Oligonucleotide Microarray for MicroRNA Expression Analysis Based on Labeling RNA with Quantum Dot and Nanogold Probe. *Nucleic Acids Res.* **2005**, *33*, e17.
29. Zhu, J.; Feng, X. L.; Lou, J. Y.; Li, W. D.; Li, S.; Zhu, H. X.; Yang, L.; Zhang, A. P.; He, L.; Li, C. Accurate Quantification of MicroRNA *via* Single Strand Displacement Reaction on DNA Origami Motif. *PLoS One* **2013**, *8*, e69856.
30. Wang, D.; Hu, L.; Zhou, H.; Abdel-Halim, E. S.; Zhu, J.-J. Molecular Beacon Structure Mediated Rolling Circle Amplification for Ultrasensitive Electrochemical Detection of MicroRNA Based on Quantum Dots Tagging. *Electrochem. Commun.* **2013**, *33*, 80–83.
31. Zhu, W.; Su, X.; Gao, X.; Dai, Z.; Zou, X. A Label-Free and PCR-Free Electrochemical Assay for Multiplexed MicroRNA Profiles by Ligase Chain Reaction Coupling with Quantum Dots Barcodes. *Biosens. Bioelectron.* **2014**, *53*, 414–419.
32. Cheng, Y.; Lei, J.; Chen, Y.; Ju, H. Highly Selective Detection of MicroRNA Based on Distance-Dependent Electrochemiluminescence Resonance Energy Transfer between CdTe Nanocrystals and Au Nanoclusters. *Biosens. Bioelectron.* **2014**, *51*, 431–436.
33. Yakovchuk, P.; Protozanova, E.; Frank-Kamenetskii, M. D. Base-Stacking and Base-Pairing Contributions into Thermal Stability of the DNA Double Helix. *Nucleic Acids Res.* **2006**, *34*, 564–574.
34. Geißler, D.; Charbonnière, L. J.; Ziessel, R. F.; Butlin, N. G.; Löhmannsröben, H.-G.; Hildebrandt, N. Quantum Dot Biosensors for Ultra-Sensitive Multiplexed Diagnostics. *Angew. Chem., Int. Ed.* **2010**, *49*, 1396–1401.
35. Cai, S.; Lau, C.; Lu, J. Sequence-Specific Detection of Short-Length DNA *via* Template-Dependent Surface-Hybridization Events. *Anal. Chem.* **2010**, *82*, 7178–7184.
36. Morgner, F.; Geißler, D.; Stufler, S.; Butlin, N. G.; Löhmannsröben, H.-G.; Hildebrandt, N. A Quantum Dot-Based Molecular Ruler for Multiplexed Optical Analysis. *Angew. Chem., Int. Ed.* **2010**, *49*, 7570–7574.
37. Steer, C. J.; Subramanian, S. Circulating MicroRNAs as Biomarkers: A New Frontier in Diagnostics. *Liver Transpl.* **2012**, *18*, 265–269.
38. Geißler, D.; Stufler, S.; Löhmannsröben, H.-G.; Hildebrandt, N. Six-Color Time-Resolved Förster Resonance Energy Transfer for Ultrasensitive Multiplexed Biosensing. *J. Am. Chem. Soc.* **2013**, *135*, 1102–1109.